A transversal substructuring mode matching method applied to the acoustic analysis of dissipative mufflers

J. Albelda*, F.D. Denia, M.I. Torres, F.J. Fuenmayor

Departamento de Ingeniería Mecánica y de Materiales, Universidad Politécnica de Valencia, Camino de Vera, s/n, 46022 Valencia, Spain

Abstract

To carry out the acoustic analysis of dissipative silencers with uniform cross-section, the application of the mode matching method at the geometrical discontinuities is an attractive option from a computational point of view. The consideration of this methodology assumes, in general, that the modes associated with the transversal geometry of each element with uniform cross-section are known for the excitation frequencies considered in the analysis. The calculation of the transversal modes is not, however, a simple task when the acoustic system involves perforated elements and absorbent materials. The current work presents a modal approach to calculate the transversal modes and the corresponding axial wavenumbers for dissipative mufflers of uniform (but arbitrary) cross-section. The proposed technique is based on the division of the transversal section into subdomains and the subsequent use of a substructuring procedure with two sets of modes to improve the convergence. The former set of modes fulfils the condition of zero pressure at the common boundary between transversal subdomains while the latter satisfies the condition of zero derivative in the direction normal to the boundary. The approach leads to a versatile methodology with a moderate computational effort that can be applied to mufflers commonly found in real applications. To validate the procedure presented in this work, comparisons are provided with finite element predictions and results available in the literature, showing a good agreement. In addition, the procedure is applied to an example of practical interest.
© 2007 Elsevier Ltd. All rights reserved.

1. Introduction

Absorbent materials are widely used by muffler manufacturers to provide suitable noise attenuation. These materials are usually included in liner ducts and their acoustic behaviour can be studied with simplified approaches, such as the fundamental (or least attenuated) mode model or the hypothesis of locally reacting impedance [1]. Higher order modes must be considered, however, in the calculations, depending on the transversal dimensions of the ducts and the frequency range to be modelled accurately. In this case, a three-dimensional model must be used and, since analytical solutions are only available for very simple geometries, numerical techniques, such as the finite element method [2,3] are required. Nevertheless, the high computational effort associated with three-dimensional finite element models and the difficulty to establish

---

*Corresponding author. Tel.: +34 96 3877621; fax: +34 96 3877629.

E-mail address: jalbelda@mcm.upv.es (J. Albelda).

useful and intuitive design relations between the characteristics of the muffler and its acoustic attenuation behaviour, lead to the consideration of modal solutions.

Modal methods, and particularly the mode matching method, have been successfully applied to the acoustic analysis of mufflers. This method carries out the coupling of the transversal modes by means of the proper acoustic conditions at the axial geometrical discontinuities between the components of the muffler. Åbom [4] applied this methodology to a circular expansion chamber with extended ducts and locally reacting lateral walls. He used the analytical transversal modes associated with a circular geometry but pointed out the possibility of obtaining the modal description by means of numerical techniques such as the finite element method. With the same approach, Selamet et al. [5–8] analysed the acoustic behaviour of several types of mufflers, including the concentric and eccentric circular expansion chamber, the circular flow-reversing chamber and expansion chambers with double outlet. The mode matching method can be also applied to moderately complex geometries, as shown in the work of Selamet et al. [9] in which a double chamber muffler with extended ducts is studied, and the work of Denia et al. [10], associated with an elliptical chamber with double outlet. In summary, the mode matching method has been applied to moderately complex geometries of reactive mufflers and provides an accurate solution with a suitable convergence. For mufflers involving complex cross-sections, the difficulties in obtaining the corresponding modes analytically arise and numerical methods must be employed [2,3].

In the presence of an absorbent material, some differences are found regarding the propagation of the acoustic waves. If the solid phase of the material can be assumed as infinitely rigid, only a compression wave propagates and the material can be characterized, from a macroscopic point of view, by a complex wavenumber and a complex impedance [11]. However, if the solid structure of the absorbent material has a finite stiffness, two compression waves and a shear wave propagate through the medium and the Biot's poroelastic model [12] adapted to the acoustic problem by Allard et al. [13] is usually considered. The first model is especially accurate when fibrous materials are used, while the poroelastic model, which takes into account the interaction between the solid structure and the pores, is preferred when porous materials are present. The first macroscopic model has been employed successfully in several works, the only restriction being that the type of absorbent material considered must fulfil the hypothesis of high stiffness of the solid phase. Astley and Cummings [14] studied the acoustical behaviour of a rectangular duct with liner on its four sides and mean flow by means of the finite element method. The authors observed a good agreement between the predictions and the measurements. Later, Bies et al. [15] presented a general modal scheme to compute the acoustic behaviour of ducts with arbitrary cross-section and mean flow. The work considered circular and rectangular ducts, and a number of design charts were provided. Several techniques are available to evaluate the transversal modes of the components involved in the muffler. Kirby [16] presented a simplified closed analytical solution based on approximations of the Bessel functions, for the case of a perforated dissipative circular concentric resonator in the presence of mean flown confined in the central tube, and showed the effect of the perforate porosity in the behaviour of the silencer. Later, the same author [3] proposed a more general methodology to predict the acoustic behaviour of dissipative silencers of arbitrary cross-section in presence of mean flow, based on the calculation of transversal modes by means of the finite element method and the point collocation technique to couple the modal expansions at the geometrical discontinuities. Glav [17] studied a dissipative resonator with arbitrary cross-section, but neglected the influence of mean flow. He adopted a point collocation approach for calculating the transversal modes whilst the coupling between the solutions at the interfaces was performed by the mode matching method. Recent works [18–20] have analysed the behaviour of circular dissipative mufflers considering analytical transversal modes. To provide an analytical expression for the transversal pressure field, the authors evaluated the pressure modes and wavenumbers solving the characteristic equation, which involves the transverse coupling of the acoustic fields in the duct and the chamber by proper boundary conditions at the interface.

The purpose of this work is to develop a computationally efficient modal method for the evaluation of the transversal modes and axial wavenumbers in perforated dissipative mufflers of arbitrary, but axially uniform, cross-sections. The method is based on Component Mode Synthesis and incorporates two sets of modes for the acoustic modelling of the transversal subdomains, leading to a faster convergence in comparison with other modal descriptions [21]. The authors propose, specifically, the utilization of two sets of modes satisfying, respectively, the conditions of zero normal velocity and zero pressure at the interface between subdomains
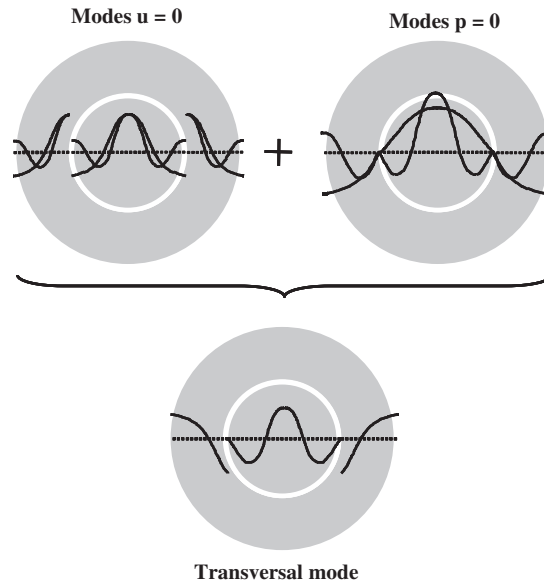
Fig. 1. Component mode synthesis scheme for calculation of transversal modes.

(Fig. 1). Previous work of the authors [22] has demonstrated the potential of this methodology in reactive configurations. It will be shown later that the use of these two sets of modes leads to an efficient approach for dissipative mufflers.

The technique proposed in this work presents some advantages in comparison with other procedures. A matrizant eigenvalue problem is finally obtained, which can be solved with commercial mathematical packages. Therefore, the technique avoids iterative schemes associated with the nonlinear eigenequation found, for instance, in the analytical modelling of perforated dissipative mufflers with circular cross-section. When solving this nonlinear eigenequation, some problems may arise, such as sensitivity of the final solution to the initial guess and modal jumping [16]. The usual significant expenditure associated with a full three-dimensional finite element model is also avoided, since the proposed methodology decouples the transverse acoustic field, thus leading to a two-dimensional problem. In addition, more useful information is obtained from a practical point of view, such as mode shapes and modal attenuation rates.

The formulation of the problem, including the governing equations, is presented in Section 2.1. The approach proposed to calculate the transversal modes of each component is derived in Section 2.2, considering a geometry that involves two arbitrary subdomains connected by a perforated tube. Section 2.3 is related to the application of the mode matching method when the transversal modes are evaluated by the finite element method. Some aspects regarding the convergence of the transversal modes are treated in Section 2.4. Finally, the method is validated by comparison with three-dimensional finite element calculations.

2. Formulation of the problem

2.1. Mathematical approach

The acoustic modelling of the muffler is carried out in this section, assuming the following hypotheses: (1) the muffler can be divided into components of uniform cross-section; (2) these components can be subdivided into disjoint subdomains connected directly or by perforated elements; (3) the medium of propagation associated with each subdomain (air or absorbent material) is defined by its acoustic impedance and wavenumber and (4) the mean flow is not considered.

In order to simplify the presentation of the component mode synthesis approach proposed to build the transversal modes, and without loss of generality, a muffler component with arbitrary but uniform
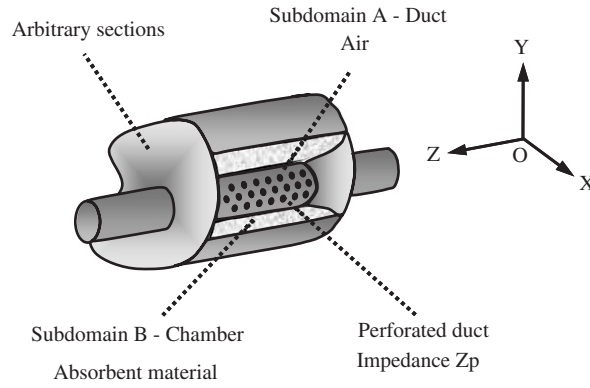
Fig. 2. Muffler and subdomains considered for the application of the component mode synthesis approach.

cross-section is considered, including two subdomains with different medium of propagation, air and absorbent material, respectively, as shown in Fig. 2.

The transversal subdomains, denoted by A and B, are connected by a perforated tube that is modelled by its acoustic impedance Z_p [1]. The axial direction of the muffler coincides with the z-axis of the Cartesian coordinate system $OXYZ$. For harmonic time variation, the propagation of sound in subdomain A, where the medium is assumed to be air, is governed by the well-known Helmholtz equation [1]

$$\nabla^2 p_A + k_0^2 p_A = 0, \tag{1}$$

∇^2 being the laplacian operator, p_A the complex amplitude of the acoustic pressure, and k_0 the wavenumber defined by ω/c_0 (where c_0 is the speed of sound and ω is the angular frequency). The acoustic wave equation in the absorbent material may be written as [11]

$$\nabla^2 p_B + \tilde{k}^2 p_B = 0, \tag{2}$$

where p_B is the amplitude of the acoustic pressure and $\tilde{k}$ is the complex wavenumber associated with the absorbent material.

Taking into account that the cross-section under consideration is uniform and using separation of variables, the amplitude of the pressure may be expressed as

$$p(x, y, z) = \Psi^{xy}(x, y) e^{-jk_z z},$$
$$\Psi^{xy}(x, y) = \begin{cases} \Psi_A^{xy}(x, y), & (x, y) \in A, \\ \Psi_B^{xy}(x, y), & (x, y) \in B, \end{cases} \tag{3}$$

where Ψ^{xy} denotes the transversal mode and k_z is the axial wavenumber. If a suitable definition of the transversal mode in each subdomain is used, Eq. (3) is valid for any point of the cross-section. Introducing Eq. (3) in Eqs. (1) and (2), associated with the air and the absorbent material, respectively, yields

$$\nabla^2 \Psi_A^{xy} + (k_0^2 - k_z^2)\Psi_A^{xy} = 0, \tag{4}$$

$$\nabla^2 \Psi_B^{xy} + (\tilde{k}^2 - k_z^2)\Psi_B^{xy} = 0. \tag{5}$$

Using the common axial wavenumber k_z and the wavenumbers of the air and the absorbent material, k_0 and $\tilde{k}$, the transversal wavenumbers in each subdomain $k_{A,t}$ and $k_{B,t}$ can be defined as

$$k_{A,t} = \pm\sqrt{k_0^2 - k_z^2}, \tag{6}$$

$$\tilde{k}_{B,t} = \pm\sqrt{\tilde{k}^2 - k_z^2}, \tag{7}$$

and therefore the following equations are satisfied:

$$\nabla^2 \Psi_A^{xy} + k_{A,t}^2 \Psi_A^{xy} = 0, \tag{8}$$

$$\nabla^2 \Psi_B^{xy} + \tilde{k}_{B,t}^2 \Psi_B^{xy} = 0. \tag{9}$$

The eigenproblem associated with the calculation of the axial wavenumbers and the corresponding transversal modes is formulated in the next section.

Once the axial wavenumbers and the transversal modes of the complete cross-section are known, the pressure field in the component under analysis can be expressed in terms of a series expansion

$$p(x,y,z) = \sum_{s=0}^{\infty} (C_s^+ e^{-jk_{z,s}^+ z} \Psi_s^{xy+} + C_s^- e^{-jk_{z,s}^- z} \Psi_s^{xy-}), \tag{10}$$

where $k_{z,s}^+$ and $k_{z,s}^-$ are the axial wavenumbers of the incident and reflected waves in the component, and C_s^+ and C_s^- are the corresponding wave coefficients.

2.2. Calculation of the transversal modes

To obtain the modes of the complete cross-section for the considered muffler component, the characteristic equations of each component, Eqs. (4) and (5), must be solved taking into account the rigid wall boundary conditions as well as those conditions related to the interface between subdomains. In this work, it is assumed that both transversal subdomains are connected by a perforated duct characterized by the acoustic impedance Z_p that relates the jump of pressure between subdomains with the acoustic velocity normal to the interface.

The transversal pressure in each subdomain Ψ_A^{xy} and Ψ_B^{xy} can be expressed considering a set of modes associated with the corresponding subdomains. The number of modes to provide an accurate pressure field depends on the boundary condition to be satisfied. Here, two sets of modes are included in the representation of the transversal pressure of each subdomain. The first set is obtained considering zero normal acoustic velocity at the interface, and the second set is calculated considering a zero pressure boundary condition at the interface. A scheme of this approach was previously depicted in Fig. 1. These two sets of modes may be evaluated analytically in the case of circular cross-sections, which are widely used in automotive industry, while a numerical calculation is in general required for more complex transversal geometries. Finally, the transversal solution in each subdomain may be expressed as

$$\Psi_A^{xy} = \sum_{r=0}^{\infty} \phi_{A,r}^{xy,u} q_{A,r}^u + \sum_{r=1}^{\infty} \phi_{A,r}^{xy,p} q_{A,r}^p, \tag{11}$$

$$\Psi_B^{xy} = \sum_{r=0}^{\infty} \phi_{B,r}^{xy,u} q_{B,r}^u + \sum_{r=1}^{\infty} \phi_{B,r}^{xy,p} q_{B,r}^p, \tag{12}$$

where $\phi_{A,r}^{xy,u}, \phi_{B,r}^{xy,u}$ and $\phi_{A,r}^{xy,p}, \phi_{B,r}^{xy,p}$ are the pressure modes of the bases obtained for each subdomain with zero normal velocity and zero pressure boundary conditions at the interface, respectively, and $q_{A,r}^u, q_{A,r}^p$ and, $q_{B,r}^u, q_{B,r}^p$ are the modal participation factors.

From a practical point of view, the expansions must be truncated and only N_A^u, N_B^u zero velocity and N_A^p, N_B^p zero pressure modes will be considered. Denoting by $N_A = N_A^u + N_A^p$ and $N_B = N_B^u + N_B^p$, Eqs. (11) and (12) may be expressed by

$$\Psi^{xy}(x,y) = \begin{cases} \sum_{r=0}^{N_A} \phi_{A,r}^{xy}(x,y) q_{A,r} = \mathbf{\Phi}_A^{\mathrm{T}} \cdot \mathbf{q}_A & (x,y) \in A, \\ \sum_{r=0}^{N_B} \phi_{B,r}^{xy}(x,y) q_{B,r} = \mathbf{\Phi}_B^{\mathrm{T}} \cdot \mathbf{q}_B & (x,y) \in B. \end{cases} \tag{13}$$

Note here that the participation factors of each subdomain must be obtained to define the associated transversal mode. The method of weighted residuals in combination with the Galerkin method is applied to

Eqs. (4) and (5) to calculate the axial wavenumbers and their transversal modes. Multiplying Eq. (4) by the transversal modes and integrating over A, the weighted residual is

$$(k_0^2 - k_z^2) \int_{\Omega_A} \Psi_A^{xy} \Psi_A^{xy} \, d\Omega + \int_{\Omega_A} \Psi_A^{xy} \nabla^2 \Psi_A^{xy} \, d\Omega = 0. \tag{14}$$

Applying the Green's theorem to Eq. (14) yields

$$(k_0^2 - k_z^2) \int_{\Omega_A} \Psi_A^{xy} \Psi_A^{xy} \, d\Omega - \int_{\Omega_A} (\nabla \Psi_A^{xy})^{\mathrm{T}} \nabla \Psi_A^{xy} \, d\Omega = -\int_{\Gamma_I} \Psi_A^{xy} \frac{\partial \Psi_A^{xy}}{\partial n} \, d\Gamma. \tag{15}$$

Both sets of modes are selected to satisfy the rigid wall condition at the outer boundary and, therefore, the integral on the right hand side is extended only to the interface Γ_I where the normal velocity is not zero. The impedance associated with the perforated duct must be considered to evaluate this term. Using Euler's equation, the normal pressure gradient at the perforated surface may be written as

$$\frac{\partial \Psi_A^{xy}}{\partial n} = -\rho_0 \frac{\partial u_{An}}{\partial t} = -\rho_0 \omega \mathrm{j} u_{An}, \tag{16}$$

where u_{An} is the amplitude of the normal velocity at the interface.

From the definition of the perforate impedance, the following relation is satisfied:

$$Z_p = \frac{\Psi_A^{xy} - \Psi_B^{xy}}{u_{An}}, \tag{17}$$

and therefore the normal velocity in Eq. (16) can be eliminated by means of Eq. (17), giving

$$\frac{\partial \Psi_A^{xy}}{\partial n} = -\rho_0 \omega \mathrm{j} \frac{\Psi_A^{xy} - \Psi_B^{xy}}{Z_p}. \tag{18}$$

The substitution of the pressure fields given by Eq. (13) in Eq. (18) yields

$$\frac{\partial \Psi_A^{xy}}{\partial n} = -\frac{\rho_0 \omega \mathrm{j}}{Z_p} \left(\mathbf{\Phi}_A^{\mathrm{T}} \cdot \mathbf{q}_A - \mathbf{\Phi}_B^{\mathrm{T}} \cdot \mathbf{q}_B \right). \tag{19}$$

Finally, Eqs. (13) and (19) can be introduced in Eq. (15) leading to

$$(k_z^2 - k_0^2) \int_{\Omega_A} \mathbf{\Phi}_A \mathbf{\Phi}_A^{\mathrm{T}} \mathbf{q}_A \, d\Omega + \int_{\Omega_A} (\mathbf{\Phi}_A \nabla)^{\mathrm{T}} (\mathbf{\Phi}_A \nabla) \mathbf{q}_A \, d\Omega$$
$$= -\frac{\rho_0 \omega \mathrm{j}}{Z_p} \int_{\Gamma_I} \mathbf{\Phi}_A (\mathbf{\Phi}_A^{\mathrm{T}} \cdot \mathbf{q}_A - \mathbf{\Phi}_B^{\mathrm{T}} \cdot \mathbf{q}_B) \, d\Gamma. \tag{20}$$

To get a more compact expression, the following matrices are defined

$$\mathbf{K}_\Omega^A = \int_{\Omega_A} (\mathbf{\Phi}_A \nabla)^{\mathrm{T}} (\mathbf{\Phi}_A \nabla) \, d\Omega, \quad \mathbf{M}_\Gamma^{A,A} = \int_{\Gamma_I} \mathbf{\Phi}_A \mathbf{\Phi}_A^{\mathrm{T}} \, d\Gamma,$$
$$\mathbf{M}_\Omega^A = \int_{\Omega_A} \mathbf{\Phi}_A \mathbf{\Phi}_A^{\mathrm{T}} \, d\Omega, \qquad \mathbf{M}_\Gamma^{A,B} = \int_{\Gamma_I} \mathbf{\Phi}_A \mathbf{\Phi}_B^{\mathrm{T}} \, d\Gamma, \tag{21}$$

and after some manipulation, Eq. (20) can be expressed as

$$(\mathbf{K}_\Omega^A - k_0^2 \mathbf{M}_\Omega^A + k_z^2 \mathbf{M}_\Omega^A) \mathbf{q}_A = \frac{\rho_0 \omega \mathrm{j}}{Z_p} (\mathbf{M}_\Gamma^{A,A} \mathbf{q}_A - \mathbf{M}_\Gamma^{A,B} \mathbf{q}_B). \tag{22}$$

In compact form

$$(\mathbf{KA}^A + k_z^2 \mathbf{MA}^A) \mathbf{q}_A + \mathbf{KA}^{A,B} \mathbf{q}_B = 0, \tag{23}$$

where

$$\mathbf{KA}^A = \mathbf{K}_\Omega^A - k_0^2 \mathbf{M}_\Omega^A + \frac{\rho_0 \omega \mathrm{j}}{Z_p} \mathbf{M}_\Gamma^{A,A}, \quad \mathbf{KA}^{A,B} = -\frac{\rho_0 \omega \mathrm{j}}{Z_p} \mathbf{M}_\Gamma^{A,B}, \quad \mathbf{MA}^A = \mathbf{M}_\Omega^A. \tag{24}$$

A similar procedure may be applied to Eq. (5). From Euler's equation, the normal pressure gradient at the perforated surface in the absorbent material (subdomain B) can be expressed as

$$\frac{\partial \Psi_B^{xy}}{\partial n} = -\tilde{\rho}\frac{\partial u_{Bn}}{\partial t} = -\tilde{\rho}\omega \mathrm{j} u_{Bn}, \tag{25}$$

where $\tilde{\rho}$ is the complex density associated with the absorbent material and u_{Bn} is the amplitude of the normal velocity at the interface. Assuming continuity of velocity at the perforated interface and taking into account that the unit vectors in the direction normal to the interface of both regions are opposite, gives

$$\frac{\partial \Psi_B^{xy}}{\partial n} = -\tilde{\rho}\omega \mathrm{j}\frac{\Psi_B^{xy} - \Psi_A^{xy}}{Z_p}. \tag{26}$$

Operating in a similar way, the corresponding equation for subdomain B can be expressed as

$$\mathbf{KA}^{B,A}\mathbf{q}_A + (\mathbf{KA}^B + k_z^2\mathbf{MA}^B)\mathbf{q}_B = 0, \tag{27}$$

with

$$\mathbf{KA}^B = \mathbf{K}_\Omega^B - \tilde{k}^2\mathbf{M}_\Omega^B + \frac{\tilde{\rho}\omega \mathrm{j}}{Z_p}\mathbf{M}_\Gamma^{B,B},$$

$$\mathbf{KA}^{B,A} = -\frac{\tilde{\rho}\omega \mathrm{j}}{Z_p}\mathbf{M}_\Gamma^{B,A},$$

$$\mathbf{MA}^B = \mathbf{M}_\Omega^B,$$

$$\mathbf{K}_\Omega^B = \int_{\Omega_B}(\mathbf{\Phi}_B\nabla)^{\mathrm{T}}(\mathbf{\Phi}_B\nabla)\,\mathrm{d}\Omega,$$

$$\mathbf{M}_\Omega^B = \int_{\Omega_B}\mathbf{\Phi}_B\mathbf{\Phi}_B^{\mathrm{T}}\,\mathrm{d}\Omega,$$

$$\mathbf{M}_\Gamma^{B,A} = \int_{\Gamma_I}\mathbf{\Phi}_B\mathbf{\Phi}_A^{\mathrm{T}}\,\mathrm{d}\Gamma,$$

$$\mathbf{M}_\Gamma^{B,B} = \int_{\Gamma_I}\mathbf{\Phi}_B\mathbf{\Phi}_B^{\mathrm{T}}\,\mathrm{d}\Gamma. \tag{28}$$

Eqs. (23) and (27) can be expressed in matrix form as

$$\left[\begin{pmatrix} \mathbf{KA}^A & \mathbf{KA}^{A,B} \\ \mathbf{KA}^{B,A} & \mathbf{KA}^B \end{pmatrix} + k_z^2\begin{pmatrix} \mathbf{MA}^A & \mathbf{0} \\ \mathbf{0} & \mathbf{MA}^B \end{pmatrix}\right]\begin{Bmatrix} \mathbf{q}_A \\ \mathbf{q}_B \end{Bmatrix} = \begin{Bmatrix} \mathbf{0} \\ \mathbf{0} \end{Bmatrix}, \tag{29}$$

and compacting the notation yields

$$(\mathbf{KA} + k_z^2\mathbf{MA})\mathbf{q} = \mathbf{0}. \tag{30}$$

Eq. (30) is associated with a standard matrizant eigenproblem defined for each frequency of excitation ω, where the eigenvalues represent the axial wavenumbers and the eigenvectors are the participation factors of the modal bases of each subdomain in the transversal mode of the complete cross-section. Since the modal expansion of the transversal mode has been truncated to solve the problem, the solution is approximated. Obviously a convergence of the pressure expansion to the real solution is expected when the number of modes is increased. The error in the evaluation of the axial wavenumbers and the participation factors depends on the number of modes employed in each subdomain (N_A and N_B, respectively). From a mathematical point of view, the maximum number of transversal modes that can be calculated depends on the number of equations considered, that is, the number of modes of the bases used in each subdomain.

2.3. Mode matching method with numerical transversal modal bases

The calculation of the transversal modes with the proposed method requires the previous computation of two modal bases for each subdomain. These modal bases can be evaluated analytically if the geometry of the

subdomains is relatively simple, leading to a straightforward computation of the integrals defined in Eqs. (21) and (28). For transversal subdomains with complex geometry, however, the calculation of the modal bases requires the application of a numerical technique such as the finite element method. Note here that this is specially suitable in this case since the integrals expressed in Eqs. (21) and (28) can be evaluated by means of the stiffness and mass matrices, as shown next.

The application of the finite element method to Eq. (8) leads to the eigenproblem [23]

$$(\mathbf{K}_A + k_0^2 \mathbf{M}_A)\, \boldsymbol{\varphi}_A = \mathbf{0}. \tag{31}$$

The mass and stiffness matrices defined in Eq. (31) can be computed by the expressions

$$\mathbf{M}_A = \sum_e \int_{\Omega^e} \mathbf{N}\mathbf{N}^{\mathrm{T}}\, \mathrm{d}\Omega, \tag{32}$$

$$\mathbf{K}_A = \sum_e \int_{\Omega^e} \mathbf{B}\mathbf{B}^{\mathrm{T}}\, \mathrm{d}\Omega, \tag{33}$$

$\mathbf{N}$ and $\mathbf{B}$ being the shape functions and their spatial derivatives, respectively. If $\boldsymbol{\varphi}_{A,k}$ denotes the kth eigenvector of the problem expressed in Eq. (31), then the associated mode is given by

$$\phi_{A,k}^{xy} = \mathbf{N}^{\mathrm{T}} \cdot \boldsymbol{\varphi}_{A,k}. \tag{34}$$

The element of the mass matrix $(\mathbf{M}_\Omega^A)_{i,j}$ defined in Eq. (21) may be evaluated by

$$(\mathbf{M}_\Omega^A)_{i,j} = \int_{\Omega_A} \boldsymbol{\Phi}_{A,i}\boldsymbol{\Phi}_{A,j}^{\mathrm{T}}\, \mathrm{d}\Omega = \boldsymbol{\varphi}_{A,i}^{\mathrm{T}} M_A \boldsymbol{\varphi}_{A,j}. \tag{35}$$

It can be observed that the evaluation of $\mathbf{M}_\Omega^A$ involves the use of the global mass matrix corresponding to the finite element method $\mathbf{M}_A$ and therefore no additional integration is required. In addition, an element $(\mathbf{K}_\Omega^A)_{i,j}$ of the stiffness matrix can be computed using the expression

$$(\mathbf{K}_\Omega^A)_{i,j} = \int_{\Omega_A} (\boldsymbol{\Phi}_A \nabla)^{\mathrm{T}} (\boldsymbol{\Phi}_A \nabla)\, \mathrm{d}\Omega = \boldsymbol{\varphi}_{A,i}^{\mathrm{T}} \mathbf{K}_A \boldsymbol{\varphi}_{A,j}. \tag{36}$$

To calculate the elements of the matrices $(\mathbf{M}_\Gamma^{A,A})_{i,j}$ and $(\mathbf{M}_\Gamma^{A,B})_{i,j}$ associated with the boundary integrals it is convenient to define conformal meshes between the two connected subdomains. In this case,

$$
\begin{aligned}
(\mathbf{M}_\Gamma^{A,A})_{i,j} &= \int_{\Omega_A} \boldsymbol{\Phi}_A \boldsymbol{\Phi}_A^{\mathrm{T}}\, \mathrm{d}\Omega = \boldsymbol{\varphi}_{A,i}^{\mathrm{T}} \mathbf{PA}_A \boldsymbol{\varphi}_{A,j}, \\
(\mathbf{M}_\Gamma^{A,B})_{i,j} &= \int_{\Gamma_1} \boldsymbol{\Phi}_A \boldsymbol{\Phi}_B^{\mathrm{T}} \mathrm{d}\Gamma = \boldsymbol{\varphi}_{A,i}^{\mathrm{T}} \mathbf{PA}_A \boldsymbol{\varphi}_{B,j},
\end{aligned}
\tag{37}
$$

where

$$\mathbf{PA}_A = \sum_e \int_{\Gamma^e} \mathbf{N}\mathbf{N}^{\mathrm{T}}\, \mathrm{d}\Gamma. \tag{38}$$

The matrices required to obtain the modes of the cross-section may be calculated with Eqs. (35)–(37). Since these results depend on the stiffness, mass and $\mathbf{PA}$ matrices of the finite element eigenproblem previously computed to obtain the modal bases in each region, the computational effort is reduced.

The muffler shown in Fig. 3 illustrates the applicability of the proposed methodology. It is assumed that the transversal modes of component 3 have been obtained with the method described above. Therefore, the acoustic pressure field in this component is given by

$$
\begin{aligned}
p_{3A} &= \sum_{s=0}^{N_3} (C_{3,s}^+ \mathrm{e}^{-\mathrm{j}k_{3,z,s}^+ z} \Psi_{3A,s}^{xy+} + C_{3,s}^- \mathrm{e}^{-\mathrm{j}k_{3,z,s}^- z} \Psi_{3A,s}^{xy-}), \\
p_{3B} &= \sum_{s=0}^{N_3} (C_{3,s}^+ \mathrm{e}^{-\mathrm{j}k_{3,z,s}^+ z} \Psi_{3B,s}^{xy+} + C_{3,s}^- \mathrm{e}^{-\mathrm{j}k_{3,z,s}^- z} \Psi_{3B,s}^{xy-}),
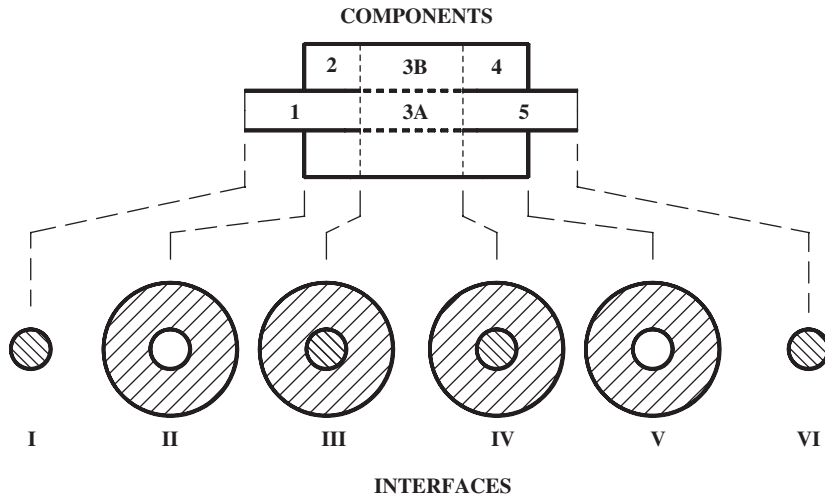\end{aligned}
\tag{39}
$$

COMPONENTS

Fig. 3. Geometry of muffler under analysis.

where the expansion has been truncated up to N_3 component modes. There is no initial distinction between progressive and regressive modes, and therefore all the modes in the bases considered for each complete transversal mode must be included. Introducing a new notation, the pressure fields are

$$p_{3A} = \sum_{s=0}^{2N_3+1} C_{3,s} e^{-jk_{3,z,s}z} \Psi_{3A,s}^{xy}, \tag{40}$$

$$p_{3B} = \sum_{s=0}^{2N_3+1} C_{3,s} e^{-jk_{3,z,s}z} \Psi_{3B,s}^{xy}. \tag{41}$$

The same considerations can be made regarding the axial acoustic velocity of component 3, that can then be determined as

$$u_{3A,z} = \frac{-1}{j\rho_0\omega} \sum_{s=0}^{2N_3+1} k_{3,z,s} C_{3,s} e^{-jk_{3,z,s}z} \Psi_{3A,s}^{xy}, \tag{42}$$

$$u_{3B,z} = \frac{-1}{j\tilde{\rho}\omega} \sum_{s=0}^{2N_3+1} k_{3,z,s} C_{3,s} e^{-jk_{3,z,s}z} \Psi_{3B,s}^{xy}. \tag{43}$$

The acoustic pressure and axial velocity fields associated with the rest of components included in the muffler are given by

$$
\begin{aligned}
p_i &= \sum_{s=0}^{2N_1+1} C_{i,s} e^{-jk_{i,z,s}z} \Psi_{i,s}^{xy}, & i &= 1,2,4,5, \\
u_{i,z} &= \frac{-1}{j\rho_i\omega} \sum_{s=0}^{2N_1+1} k_{i,z,s} C_{i,s} e^{-jk_{i,z,s}z} \Psi_{i,s}^{xy}, & i &= 1,2,4,5, \\
\rho_i &= \begin{cases} \rho_0, & i = 1,5, \\ \tilde{\rho}, & i = 2,4, \end{cases}
\end{aligned}
\tag{44}
$$

where the wavenumbers of each component are expressed as follows:

$$k_{i,z,s} = \sqrt{k_i^2 - k_{i,t}^2}, \quad i = 1, 2, 4, 5,$$

$$k_i = \begin{cases} k_0, & i = 1, 5, \\ \tilde{k}, & i = 2, 4. \end{cases} \tag{45}$$

The transversal wavenumbers of the components can be obtained solving the following eigenproblem with the corresponding boundary conditions:

$$\Delta \Psi_i^{xy} + k_{i,t}^2 \Psi_i^{xy} = 0, \quad i = 1, 2, 4, 5. \tag{46}$$

To solve the acoustic problem in the muffler, all wave coefficients $C_{i,s}$ for $i = 1, \ldots, 5$, must be computed. This task is performed using the mode matching method, which couples the acoustic fields at the geometrical discontinuities [4] by means of the boundary conditions shown in Table 1. For the computation of the integrals associated with the mode matching technique, the mass matrix considered earlier in the finite element calculation of the modal bases can be employed, as shown next.

The transversal modes of the component 3 defined in Eq. (13) may be expressed as

$$\Psi_{3,s}^{xy}(x,y) = \begin{cases} \mathbf{\Phi}_{3A}^{\mathrm{T}} \cdot \mathbf{q}_{3A,s}, & (x,y) \in 3A, \\ \mathbf{\Phi}_{3B}^{\mathrm{T}} \cdot \mathbf{q}_{3B,s}, & (x,y) \in 3B. \end{cases} \tag{47}$$

The multiplication of two arbitrary modes yields

$$\Psi_{3,i}^{xy}(x,y)\Psi_{3,j}^{xy}(x,y) = \begin{cases} (\mathbf{q}_{3A,i})^{\mathrm{T}} \mathbf{\Phi}_{3A} \mathbf{\Phi}_{3A}^{\mathrm{T}} \mathbf{q}_{3A,j}, & (x,y) \in 3A, \\ (\mathbf{q}_{3B,i})^{\mathrm{T}} \mathbf{\Phi}_{3B} \mathbf{\Phi}_{3B}^{\mathrm{T}} \mathbf{q}_{3B,j}, & (x,y) \in 3B, \end{cases} \tag{48}$$

Table 1
Type of boundary conditions at the interface between components of the muffler

Section	Boundary condition	Type of boundary condition
I	$p_1 = 1, \quad (x,y) \in \Gamma_{\mathrm{I}}$	Pressure continuity
II	$\vec{u}_2 \cdot \vec{n} = 0, \quad (x,y) \in \Gamma_{\mathrm{II}}$	Rigid wall
III	$p_1 = p_{3A}, \quad (x,y) \in \Gamma_{\mathrm{III}A}$	Pressure continuity
	$p_2 = p_{3B}, \quad (x,y) \in \Gamma_{\mathrm{III}B}$	Pressure continuity
	$(\vec{u}_1 + \vec{u}_2 + \vec{u}_3) \cdot \vec{n} = 0,$ $(x,y) \in \Gamma_{\mathrm{III}}$	Compatibility of velocity
IV	$p_{3A} = p_5, \quad (x,y) \in \Gamma_{\mathrm{IV}A}$	Pressure continuity
	$P_{3B} = P_5, \quad (x,y) \in \Gamma_{\mathrm{IV}B}$	Pressure continuity
	$(\vec{u}_3 + \vec{u}_4 + \vec{u}_5) \cdot \vec{n} = 0,$ $(x,y) \in \Gamma_{\mathrm{IV}}$	Compatibility of velocity
V	$\vec{u}_4 \cdot \vec{n} = 0, \quad (x,y) \in \Gamma_{\mathrm{V}}$	Rigid wall
VI	$p_5 = \rho_0 c_0 \vec{u} \cdot \vec{n}, \quad (x,y) \in \Gamma_{\mathrm{VI}}$	Anechoic termination

and the integration over the cross-section leads to

$$\int_{\Gamma_{IV}} \Psi_{3,i}^{xy} \Psi_{3,j}^{xy} \, d\Gamma = (\mathbf{q}_{3A,i})^{\mathrm{T}} \mathbf{M}_{\Omega}^{3A} \mathbf{q}_{3A,j} + (\mathbf{q}_{3B,i})^{\mathrm{T}} \mathbf{M}_{\Omega}^{3B} \mathbf{q}_{3B,j}, \tag{49}$$

where the elements of the matrices $\mathbf{M}_{\Omega}^{3A}, \mathbf{M}_{\Omega}^{3B}$ are obtained by means of Eq. (35) from the mass matrix previously calculated with the finite element method.

For a muffler component with simple cross-section, the transversal modes can be evaluated analytically, and therefore the integral on the left-hand side of Eq. (49) is easily computed. This is the case of a wide variety of commercial mufflers that involve circular ducts, for which the transversal modes are known.

2.4. Considerations about the transversal modes

The weighted residual method has been employed in the previous section to obtain the transversal modes, and therefore the resulting axial wavenumbers are approximated. The fulfilment of the boundary conditions associated with the perforated tube is only enforced in a weak way and consequently the pressure given by the procedure is not exact. To illustrate the convergence of the modal solution, some studies are carried out in this section related to the transversal modes provided by the proposed method. The simple circular concentric resonator with absorbent material presented by Cummings and Chang [24] is considered. In this example, the perforated pipe is not included in the analysis, and the outer and inner radii are $R_2 = 0.038$ m and $R_1 = 0.0198$ m, respectively. The model and data of the absorbent material are those considered in the work of Cummings and Chang.

Fig. 4 shows the modulus of the transversal modes computed with the proposed method, the frequency being 3 kHz. The calculations have been carried out considering 12 modes (6 modes associated with the zero pressure condition at the interface and 6 modes for the zero velocity condition). The transversal modes depicted have been normalized as in Ref. [24], with a maximum value equal to unity. It is found that the results provided by the technique proposed here and those obtained by Cummings and Chang are in good agreement.

The convergence of the transversal modal solution is illustrated in Fig. 5, where the effect of increasing the number of zero pressure and zero velocity basic modes is shown. It can be seen that the convergence is adequate, since the solutions obtained with 12 and 16 basic modes are essentially identical. The participation
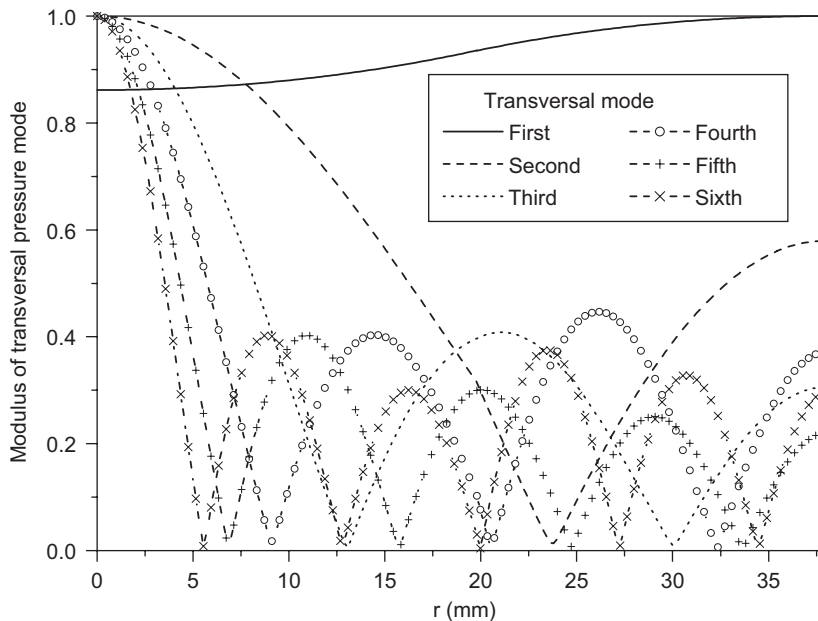
Fig. 4. Modulus of transversal pressure modes for frequency of excitation of 3 kHz. — first mode, - - - second mode, ... third mode, - ○ - fourth mode, - + - fifth mode, - × - sixth mode.
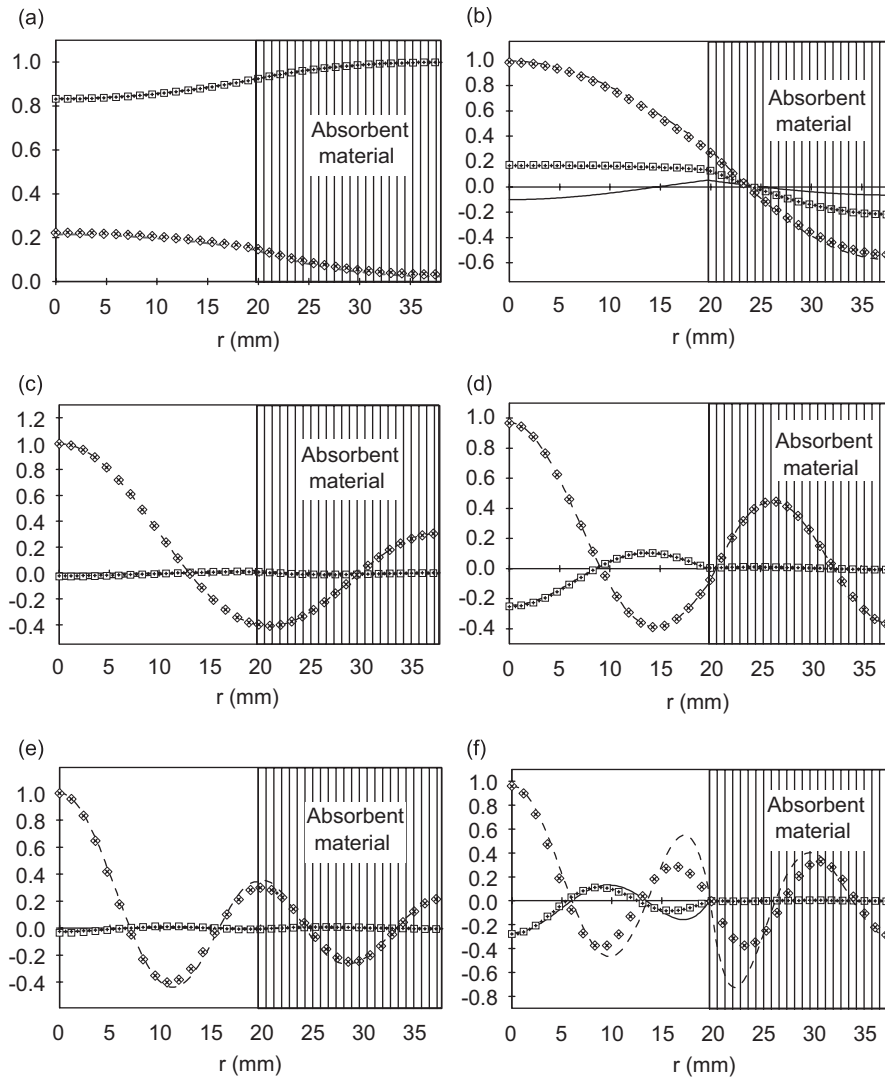
Fig. 5. Transversal pressure modes for frequency of excitation of 3 kHz: (a) first mode, (b) second mode, (c) third mode, (d) fourth mode, (e) fifth mode, (f) sixth mode: —, real part, 8 basic modes; □ □ □, real part, 12 basic modes; + + +, real part, 16 basic modes; - - -, imaginary part, 8 basic modes; ◇ ◇ ◇, imaginary part, 12 basic modes; × × ×, imaginary part, 16 basic modes.

factors of the zero pressure and zero velocity basic modes are depicted in Fig. 6, for the fundamental and second least attenuated transversal modes. It is found a rapid convergence as the number of modes increases, thus confirming the validity of the current approach.

3. Results and discussion

To check the accuracy of the proposed procedure, Fig. 7 shows the transmission loss associated with the dissipative muffler considered by Cummings and Chang [24]. For comparison purposes, the results given by the proposed procedure, as well as those from the method described in Ref. [24] and three-dimensional finite element calculations, are included in the figure, the latter being obtained by the commercial program SYSNOISE. For the current geometry and frequency range of interest, all three sets are in good agreement, supporting the potential use of the method proposed here for the analysis of dissipative mufflers.

(a)

(b)

(c)

(d)
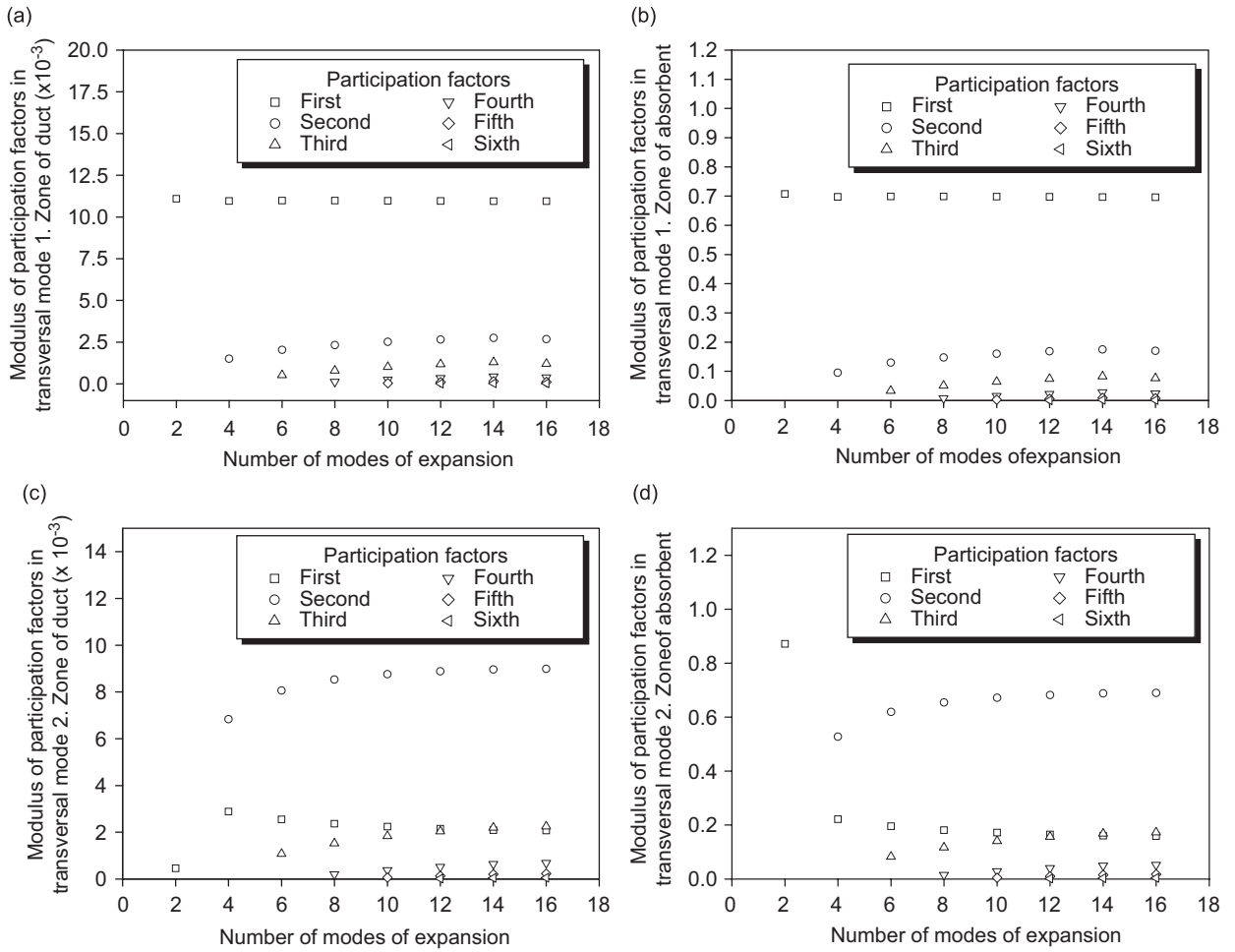
Fig. 6. Participation factors of the transversal pressure modes for a frequency of excitation of 3 kHz: (a) modes in duct for first transversal mode, (b) modes in absorbent for first transversal mode, (c) modes in duct for second transversal mode, (d) modes in absorbent for second transversal mode; □ □ □, first basic mode, ○ ○ ○, second basic mode, △ △ △, third basic mode, ▽ ▽ ▽, fourth basic mode, ◇ ◇ ◇, fifth basic mode, ◁ ◁ ◁, sixth basic mode.
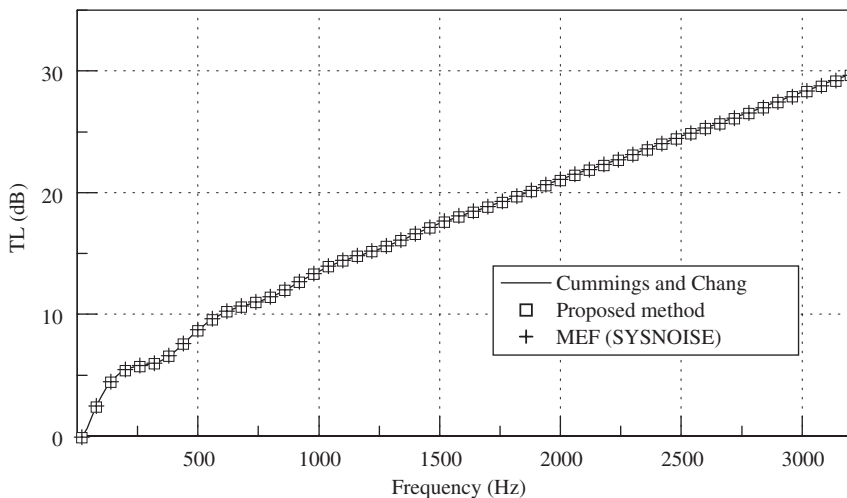
Fig. 7. TL for circular concentric resonator. —, Cummings and Chang [24]; □ □ □, proposed method; + + +, FEM.
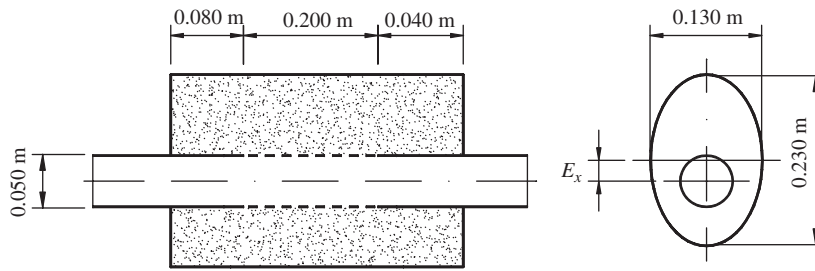
Fig. 8. Muffler considered to analyse the effect of the offset of the perforated duct.

Table 2
Offset distances for the perforated dissipative elliptical resonator with offset extended inlet/outlet

Silencer reference	Offset distance E_x (m)
RCOVEX1	0.000
RCOVEX2	0.0339
RCOVEX3	0.0678

To illustrate the application of the proposed technique for more complex mufflers, the influence of the offset distance associated with the central passage is analysed for the perforated dissipative elliptical resonator with offset extended inlet/outlet shown in Fig. 8. Table 2 shows the offset distances considered to evaluate the behaviour of this type of muffler. The current analysis considers a low resistivity fiber defined in Appendix A, in order to obtain a clear influence of the offset distance. The use of high resistivity fiber, such as this used in Fig. 7, strongly dampens this effect, thus justifying the use of a different material in the current discussion. The impedance of the perforated tube, defined in Appendix A, incorporates the effect of the absorbent material. The hole diameter of the perforated surface is $d_h = 0.003$ m, the thickness of the tube is $t_h = 0.001$ m and the porosity is defined by $\sigma = 5\%$.

The modal bases of the transversal subdomains were computed by the finite element package SYSNOISE with the meshes shown in Fig. 9. In all the cases, quadratic quadrilateral elements are considered. Fig. 9 also displays the number of nodes of each mesh and the frequencies of the first three modes of the bases, associated with zero velocity and zero pressure at the interface between subdomains.

To clarify the combined effect of the absorbent material and the offset distance, purely reactive mufflers are considered first. For this case, the influence of the offset distance in the TL is shown in Fig. 10. In the low frequency range, the TL is similar for the three configurations due to the predominance of one-dimensional wave propagation. For higher frequencies, the propagation of higher order modes begins and the transmission loss for each muffler is different since the frequency of the transversal modes changes with the offset distance of the central duct. An increase in the offset distance is shown to lead to multidimensional propagation at lower frequencies, and therefore a worse acoustic attenuation is produced in a wide frequency range. As a consequence of the propagation of the higher order modes, the transmission loss is reduced drastically, and only in relatively narrow frequency bands keeps a reasonable value.

Fig. 11 shows the TL for the same geometries analysed in the previous figure, now including absorbent material inside the muffler. In the current case the transmission loss does not exhibit the drastic collapse associated with the propagation of higher order modes and a reasonable attenuation is obtained for frequencies below 1500 Hz. The peaks and pass bands observed in Fig. 10 have disappeared and the maximum value of the transmission loss shifts to higher frequencies when the offset is increased. This means that the maximum attenuation band between 500 and 1500 Hz can be selected by an appropriate offset distance. For high frequencies the TL seems to be independent of the position of the central perforated tube, since all the curves tend to the same value.
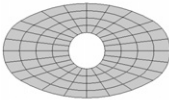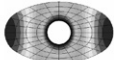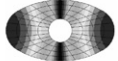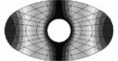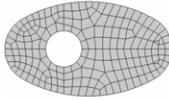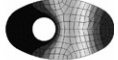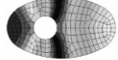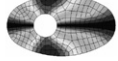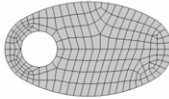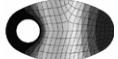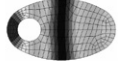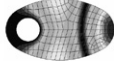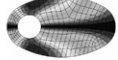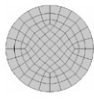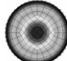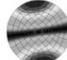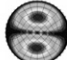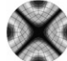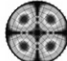
Annular chamber or central duct	f (Hz) Base u=0		f (Hz) Base p=0	
RECOVEX1 336 nodes		0		948
		756		1001
		1267		1807
RECOVEX2 665 nodes		0		714
		783		1513
		1282		1692
RECOVEX3 728 nodes		0		556
		875		1527
		1325		1581
349 nodes		0		5205
		3985		8295
		6611		11119

Fig. 9. Data associated with the meshes considered for the calculation of the transversal modal bases of annular chamber and central duct.
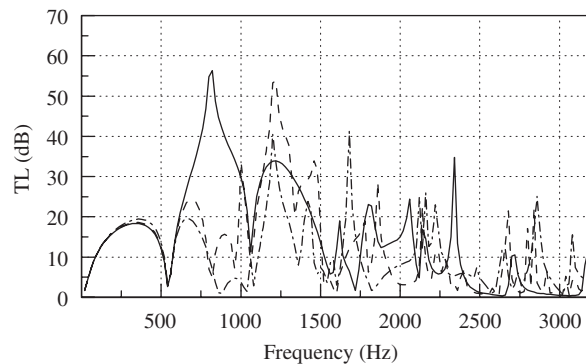

Fig. 10. TL of perforated elliptical resonator with offset extended inlet/outlet: —, RCOVEX1; - - -, RCOVEX2; · - · - · -, RCOVEX3.
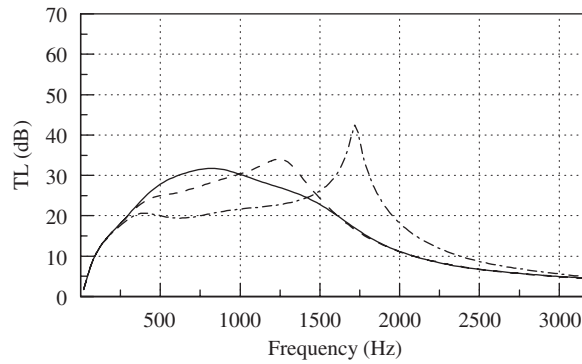
Fig. 11. TL of perforated dissipative elliptical resonator with offset extended inlet/outlet: —, RCOVEX1; - - -, RCOVEX2; ·-·-·-, RCOVEX3.

4. Concluding remarks

This work has presented a new modal method to calculate the acoustic behaviour of perforated dissipative mufflers involving ducts with arbitrary (but axially uniform) cross-section. First, the different cross-sections have been divided into disjoint subdomains. Two modal bases have been considered for each subdomain, associated with zero normal velocity and zero pressure boundary conditions at the interface between subdomains of the same cross-section. Then, the complete transversal modes have been evaluated by component mode synthesis. Finally, the mode matching method has been applied at the geometrical discontinuities to calculate the global acoustic behaviour of the muffler. The proposed methodology has been validated by comparison with three-dimensional finite element calculations. In addition, the procedure has been used for the analysis of the acoustic attenuation performance of a perforated dissipative elliptical resonator with offset extended inlet/outlet. Although no mean flow has been considered in the current work, it should be noted, however, that the approach described here may easily be extended to the mean flow case.

Acknowledgements

Appendix A. Models for the absorbent material and the perforated pipe impedance

The absorbent material model presented by Delany and Bazley [25], applied to the material characterized by Xu et al. [20] is considered. The complex wavenumber of the absorbent material is expressed as

$$\frac{\tilde{k}}{k_0} = 1 + 0.1472\left(\frac{\omega}{2\pi R}\right)^{-0.577} - j0.1734\left(\frac{\omega}{2\pi R}\right)^{-0.595}, \tag{A.1}$$

R being the flow resistivity. It is possible to define an equivalent complex speed of sound in the absorbent material by means of

$$\tilde{c} = \frac{\omega}{\tilde{k}}. \tag{A.2}$$

For the characteristic impedance of the absorbent material, the expression is

$$\frac{\tilde{Z}}{Z_0} = 1 + 0.0855\left(\frac{\omega}{2\pi R}\right)^{-0.754} - j0.0765\left(\frac{\omega}{2\pi R}\right)^{-0.732}, \tag{A.3}$$

and the equivalent complex density of the absorbent can be obtained from Eqs. (A.1)–(A.3), yielding

$$\tilde{\rho} = \frac{\tilde{Z}}{\tilde{c}} = \frac{\tilde{Z}\tilde{k}}{\omega}. \tag{A.4}$$

In this work, the resistivity of the absorbent material is $R = 4896 \, \text{rayl/m}$, associated with a density of $100 \, \text{kg/m}^3$.

To account for the presence of the absorbent material, the expression of the perforated pipe impedance is modified [26], giving

$$Z_p = \frac{\rho_0 c_0}{\sigma} \left(0.006 + \mathrm{j}k_0 \left[t_h + 0.375 d_h \left(1 + \frac{\tilde{Z}}{Z_0} \frac{\tilde{k}}{k_0} \right) \right] \right), \tag{A.5}$$

where t_h is the thickness of the perforated pipe, d_h the diameter of the orifices and σ is the porosity.

References

[1] M.L. Munjal, *Acoustics of Ducts and Mufflers*, Wiley-Interscience, New York, 1987.
[2] K.S. Peat, K.L. Rathi, A finite element analysis of the convected acoustic wave motion in dissipative silencers, *Journal of Sound and Vibration* 184 (1995) 529–545.
[3] R. Kirby, Transmission loss predictions for dissipative silencers of arbitrary cross section in the presence of mean flow, *Journal of the Acoustical Society of America* 114 (2003) 200–209.
[4] M. Åbom, Derivation of four-pole parameters including higher order mode effects for expansion chamber mufflers with extended inlet and outlet, *Journal of Sound and Vibration* 137 (1990) 403–418.
[5] A. Selamet, P.M. Radavich, The effect of length on the acoustic attenuation performance of concentric expansion chambers: an analytical, computational, and experimental investigation, *Journal of Sound and Vibration* 201 (1997) 407–426.
[6] A. Selamet, Z.L. Ji, Acoustic attenuation performance of circular expansion chambers with offset inlet/outlet: I. Analytical approach, *Journal of Sound and Vibration* 213 (1998) 601–617.
[7] A. Selamet, Z.L. Ji, Acoustic attenuation performance of circular flow-reversing chambers, *Journal of Acoustical Society of America* 104 (1998) 2867–2877.
[8] A. Selamet, Z.L. Ji, Acoustic attenuation performance of circular expansion chambers with single-inlet and double-outlet, *Journal of Sound and Vibration* 229 (2000) 3–19.
[9] A. Selamet, F.D. Denia, A.J. Besa, Acoustic behavior of circular dual-chamber mufflers, *Journal of Sound and Vibration* 265 (2003) 967–985.
[10] F.D. Denia, L. Baeza, J. Albelda, F.J. Fuenmayor, Acoustic behaviour of elliptical mufflers with single-inlet and double-outlet, *Proceedings of the 10th International Congress on Sound and Vibration*, Stockholm, July 2003, pp. 3287–3294.
[11] P.M. Morse, K.U. Ingard, *Theoretical Acoustics*, McGraw-Hill, New York, 1968.
[12] M.A. Biot, The theory of propagation of elastic waves in a fluid-saturated porous solid, *Journal of the Acoustical Society of America* 28 (1956) 168–191.
[13] J.-F. Allard, A. Aknine, C. Depollier, Acoustical properties of partially reticulated foams with high and medium flow resistance, *Journal of the Acoustical Society of America* 79 (1986) 1734–1740.
[14] R.J. Astley, A. Cummings, A finite element scheme for attenuation in ducts lined with porous material: comparison with experiments, *Journal of Sound and Vibration* 116 (1987) 239–263.
[15] D.A. Bies, C.H. Hansen, G.E. Bridges, Sound attenuation in rectangular and circular cross-section ducts with flow and bulk-reacting liner, *Journal of Sound and Vibration* 146 (1991) 47–80.
[16] R. Kirby, Simplified techniques for predicting the transmission loss of a circular dissipative silencer, *Journal of Sound and Vibration* 243 (2001) 403–426.
[17] R. Glav, The point-matching method on dissipative silencers of arbitrary cross section, *Journal of Sound and Vibration* 189 (1996) 123–135.
[18] A. Selamet, M.B. Xu, I.-J. Lee, N.T. Huff, Analytical approach for sound attenuation in perforated dissipative silencers, *Journal of the Acoustical Society of America* 115 (2004) 2091–2099.
[19] A. Selamet, M.B. Xu, I.-J. Lee, N.T. Huff, Analytical approach for sound attenuation in perforated dissipative silencers with inlet/outlet extensions, *Journal of the Acoustical Society of America* 117 (2005) 2078–2089.
[20] M.B. Xu, A. Selamet, I.-J. Lee, N.T. Huff, Sound attenuation in dissipative expansion chambers, *Journal of Sound and Vibration* 272 (2004) 1125–1133.
[21] W.L. Li, Comparison of Fourier sine and cosine series expansions for beams with arbitrary boundary conditions, *Journal of Sound and Vibration* 255 (2002) 185–194.
[22] F.J. Fuenmayor, F.D. Denia, J. Albelda, L. Baeza, A modal substructuring method for the prediction of the acoustic performance in mufflers, *Proceedings of the Forum Acusticum. 3rd European Congress on Acoustics*, Seville, September 2002.
[23] O.C. Zienkiewicz, R.L. Taylor, *The Finite Element Method. Volume 1: The Basis*, Butterworth-Heinemann, Oxford, 2000.

[24] A. Cummings, I.-J. Chang, Sound attenuation of a finite length dissipative flow duct silencer with internal mean flow in the absorbent, *Journal of Sound and Vibration* 127 (1988) 1–17.

[25] M.E. Delany, E.N. Bazley, Acoustical properties of fibrous absorbent materials, *Applied Acoustics* 3 (1970) 105–116.

[26] R. Kirby, A. Cummings, The impedance of perforated plates subjected to grazing gas flow and backed by porous media, *Journal of Sound and Vibration* 217 (1998) 619–636.